Review of Scientific Instruments

Large field of view imaging system for remote target capture and trajectory measurement based on cone rotation

Cite as: Rev. Sci. Instrum. **89**, 063704 (2018); https://doi.org/10.1063/1.5023757
Submitted: 27 January 2018 . Accepted: 24 May 2018 . Published Online: 22 June 2018

Xiang Zhang, and Yunguo Gao

Large field of view imaging system for remote target capture and trajectory measurement based on cone rotation

Xiang Zhang[1,2] and Yunguo Gao[1,a)]
[1]*Changchun Institute of Optics, Fine Mechanics and Physics, Chinese Academy of Sciences, Changchun 130033, China*
[2]*University of the Chinese Academy of Sciences, Beijing 100039, China*

(Received 27 January 2018; accepted 24 May 2018; published online 22 June 2018)

In the remote target trajectory measurement system, because of the size limitation of the image sensor, the angle of view of the current telephoto camera is very small, which cannot meet the requirements of target acquisition. After comparing the current large-field imaging methods, a scheme of a large field of view (FoV) and high frame rate scanning by controlling the camera to perform conical rotation is proposed, and a 3 × 3 external FoV stitching system that includes the scheme is designed. An experimental prototype was constructed to verify the system. In this paper, the mechanical structure of the prototype, the camera exposure control flow, and the image data processing flow are introduced, and the imaging motion feature of the prototype caused by the camera exposure during conical motion is analyzed. In the experiment, the prototype controlled the camera accurately exposed to the sub-fields. Using a camera with an angle of view of 0.78°, a large angle of view system of 2.23° was obtained by FoV stitching. The system we present is less difficult to implement and has obvious advantages in volume and weight compared to multi-camera arrays. It is suitable for engineering applications in remote target measurement system. *Published by AIP Publishing.* https://doi.org/10.1063/1.5023757

I. INTRODUCTION

In a remote target trajectory measurement task, the first need is to capture the target. One way to deal with the problem currently is using the radar to detect the target firstly, and then in the guide of radar using tracking turntable to control the telephoto camera to image the target.[1–3] However, limited to the size of the image sensor, current telephoto camera has a small field of view. In practical applications as there is a certain amount of error in the target coordinates provided by the radar, the telephoto camera's FoV cannot completely accommodate the possible range of the target, which cannot meet the capture requirement. Therefore, the telephoto camera's FoV needs to be enlarged.

The current large field imaging system mainly uses the FoV stitching method to expand the FoV, and according to the difference in the stitching modes, it can be divided into two types: internal FoV stitching and external FoV stitching.[4] The internal FoV stitching system splices multiple image sensors into an equivalent large size sensor and gets a large field image when matched with the corresponding lens. Because the edges of common sensors encapsulate the signal transmission pins, large non-photosensitive areas exist when splicing the sensors in the focal plane directly, which results in a large blind area in the camera. To address the problem, the astronomical telescope MOA-cam3's digital camera uses a special packaged CCD, the pins of which are arranged at one side so that the other three sides for the splicing side and finally the gaps between adjacent CCD photosensitive areas are decreased to 1.5 mm.[5] As this method requires specialized custom image sensors, the cost is high.[6–8] The aerial camera UltraCam splits nine common image sensors into four groups and mounts them onto four coaxial lenses' focal planes, and this prevents interference by arranging adjacent sensors into different lenses' focal planes. And by controlling the corresponding FoV of adjacent sensors that overlap a little, the camera can obtain a complete large field image.[9] The camera ARGUS-IS makes complete use of this method, and it uses a plurality of relatively inexpensive, small-sized sensors and prevents interference by installing every four adjacent sensors that forms a 2 × 2 square into 4 coaxial lenses.[10] In theory, this method can stitch any number of sensors using 4 lenses and is an ideal way to solve the problem of the small size of a single sensor. However, except for dealing with the high precision splicing of the sensors, constructing an internal FoV stitching system also needs to design large field lens. Due to the rapid increase in imaging distortion with the angle of view when widening the FoV on the basis of the existing telephoto lens, it is very difficult to design and manufacture a lens that can match such a large FoV and resolution.[11] So generally the internal FoV stitching system is difficult to be constructed.

The external FoV stitching system arranges multiple small FoV cameras in a certain way into an array to obtain large field images. The system is easy to be constructed for that it is based on the existing cameras and only the camera support structure needs to be designed. But due to the use of multiple cameras, the system is large in volume and heavy in weight.[12–14] Because in the remote target measurement task the imaging system needs to be loaded onto the tracking turntable and the cost of turntables increases exponentially with the load, the use of the multi-camera array greatly increases the cost of the entire system.[15] Another way to achieve external FoV

a)E-mail: gaoyunguo@163.com

stitching is the scanning mirror technology.[16–18] The system installs a mirror in front of the camera and realizes wide field scanning by rotating the mirror. In order to get a high quality image, the scanning mirror system generally works in a step-scanning state, that is, controlling the mirror to rotate to a certain orientation and rest, exposes the camera, and then controls the mirror to move fast to the next orientation. Because it needs to control the mirror to start-up/brake rapidly and periodically, and makes the mirror stop exactly at a specific angle, the main technical difficulties with the scanning mirror system are the lightweight design of the mirror and its high-precision motion control.[18] And the motion control difficulty further increased when the camera's angle of view is small.

This paper presents a novel external FoV stitching system that realizes continuous scanning of a large field by controlling the camera to perform conical rotation. It realizes the simulation of a multi-camera array with a few cameras. The proposed system is easy to be constructed and suitable for capturing and monitoring remote targets.

II. PRINCIPLE OF THE EXTERNAL FOV STITCHING SYSTEM

The remote target measurement system installs the telephoto camera onto the tracking turntable to capture and image the target, and then it controls the target image to the center of the camera's FoV and measures the target's orientation according to the centroid of the target image.[19] While the current telephoto camera cannot meet the target capture requirements due to the small FoV, we propose a large field scanning method that realizes large field imaging by controlling the camera to perform conical rotation. As shown in Fig. 1, the method controls the camera through a continuous conical rotation around the axis and triggers the camera when it is at a certain position to obtain four partially overlapping sub-images. Then, the sub-images are stitched into a complete large field image.

A large field remote target acquisition and measurement system shown in Fig. 2 is designed. In the figure, the No. 2 subsystem is a single camera and takes the image of the No. 5 sub-field, and two systems shown in Fig. 1 are added beside the No. 2 subsystem as the No. 1 and No. 3 subsystems. The two subsystems are arranged parallel to the No. 2 camera's optical axis, and their conical rotation vertex angles are different, so that the No. 1 subsystem images subfields 2, 4, 6 and 8, No. 3 subsystem images sub-fields 1, 3, 7, and 9. When the 9 partially overlapping images are combined, the system achieves 3 × 3 large field stitching. Figure 3(a) shows the solid schematic of the measurement system when the imaging system is installed onto the tracking turntable, and

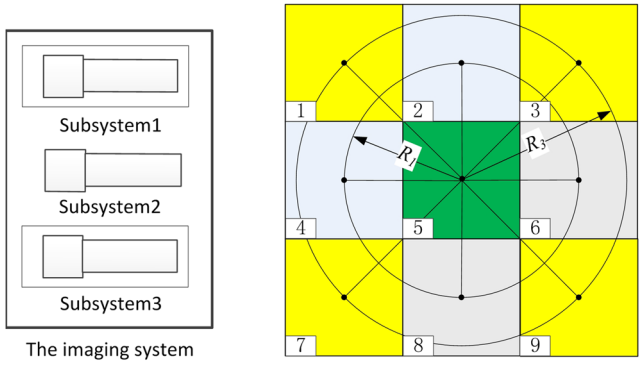

FIG. 2. Schematic diagram of 3 × 3 FoV stitching. The circles corresponding to R_1 and R_3 are, respectively, the trajectories of the camera optical axes of the No. 1 and No. 3 subsystems in the field.

Fig. 3(b) shows the sketch of the imaging system. It can be seen from the figure that the measurement system's pointing direction is the No. 2 camera's optical axis pointing direction; therefore, the No. 2 subsystem is used to measure the target trajectory, while the addition of No. 1 and No. 3 subsystems plays the role of capturing the target in a large field. Another advantage of using the No. 2 subsystem to monitor the target is that it collects better-quality images compared with No. 1 and No. 3 subsystems which capture images when the cameras are in cone motion. There is a certain degree of image motion of the images collected by No. 1 and No. 3 subsystems (see Sec. IV), which results in image ghosting and may affect the extraction of the target image centroid. When the target is captured, its image would be moved to the center of No. 2 subsystem's FoV, that is, the center of No. 5 sub-field in Fig. 2, to achieve continuous tracking and trajectory measurement of the target, while the No. 1 and No. 3 subsystems stop working.

The system's three subsystems use the same telephoto camera. Assuming that the resolution of the camera's image sensor is $n \times n$ and the overlap of the adjacent sub-images is x, then the resolution of the complete image of the system is $(3n - 2x) \times (3n - 2x)$. Suppose the pixel size is v and the focal length of the lens is f, then the camera's angle of view is $2 \cdot \arctan(\frac{\sqrt{2}n \cdot v}{2f})$, the overall angle of view of the system is $2 \cdot \arctan[\frac{\sqrt{2}(3n-2x) \cdot v}{2f}]$, and the respective conical rotation vertex angles of the No. 1 and No. 3 subsystems are

$$\begin{cases} \theta_1 = 2 \cdot \tan^{-1}\left[\dfrac{(n-x) \cdot v}{f}\right], \\ \theta_3 = 2 \cdot \tan^{-1}\left[\dfrac{\sqrt{2}(n-x) \cdot v}{f}\right]. \end{cases} \tag{1}$$

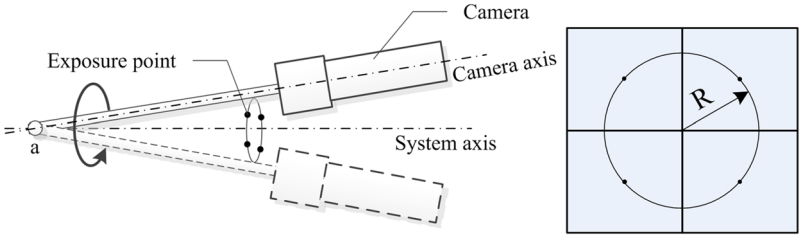

FIG. 1. Schematic diagram of the large field scanning method. The camera rotates around the system axis, while it does not rotate around the camera axis. Point a is the intersection of the camera optical axis in the running state and also the cone rotation vertex; the circle corresponding to R is the track of the optical axis in the field.

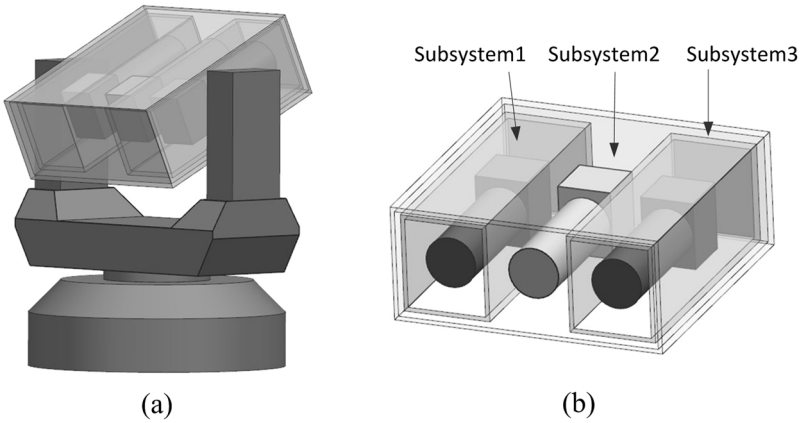

FIG. 3. (a) Schematic of the remote target measurement system and (b) sketch of the imaging system.

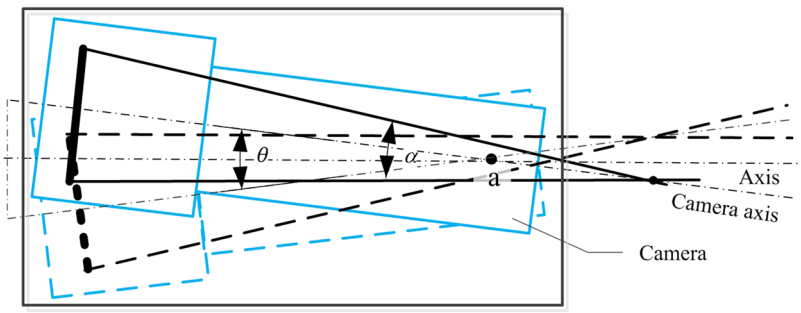

FIG. 4. Schematic of the camera's conical rotation.

An experimental prototype is designed to verify the imaging principle. Since the No. 1 and No. 3 subsystems have identical structures and make use of the same camera, just the vertex angles of conical rotation are different, only a single subsystem prototype was constructed.

III. DESIGN OF THE EXPERIMENTAL PROTOTYPE

A. Structure design of the prototype

In the camera conical rotation schematic shown in Fig. 1, the camera is at the right side of point a and is far away from point a, and its conical rotation requires a lot of space for movement, which is unfavorable to the reduction in the overall volume of the system. As shown in Fig. 4, by adjusting the position of the camera relative to point a, the minimum overall space for the movement of the camera could be obtained. In the figure, α is the angle of view of the camera and θ is the cone rotation vertex angle, that is, the angle between the optical axes when the camera is in the two extreme positions.

A spherical hinge is used to control the movement of the camera to realize the conical rotation. As shown in Fig. 5, by controlling the camera's optical axis through the center of two spherical hinges, among which the left hinge is fixed to the base with its center on the axis and the right hinge's center is at a distance from the axis, it can control the camera to perform continuous conical rotation when adding the rotary force to the rotary motion pair.

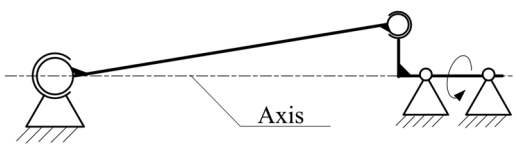

FIG. 5. Structure design schematic of the prototype.

In the prototype, a ball knuckle bearing is used as the spherical hinge. The mechanical structure shown in Fig. 6 is designed. The components of the structure are the base, left bearing seat, left knuckle bearing, camera bracket, camera, right knuckle bearing, right bearing seat, driving shaft, fine turning knob, deep groove ball bearing, bearing seat, and motor. The camera is attached to the bracket, and the bracket is held by the left and right knuckle bearings. The knuckle bearings are, respectively, installed in the corresponding bearing seats. The left bearing seat is fixed on the base, and the right bearing seat is fixed on the driving shaft and rotates with the driving shaft. The driving shaft is held by two deep groove ball bearings and provided with the rotary force by the motor. The axis of the driving shaft is taken as the system axis. The axis of the left knuckle bearing's outer ring coincides with the system axis, and the axis of the right knuckle bearing's outer ring is positioned with a certain eccentricity relative to the system axis. Thus, when the motor drives the driving shaft to rotate, the camera will perform a conical rotation with the bracket, the vertex of which is the center of the left knuckle bearing, the generatrix of which is the camera optical axis, and the axis of which is the system axis. Assuming that the conical rotation vertex angle is θ, the projection distance on the system axis between the two knuckle bearings is l, and then

$$\tan\left(\frac{\theta}{2}\right) = \frac{e}{l}. \tag{2}$$

A fine turning knob is positioned on the driving shaft and is connected to the driving shaft by a fine thread to adjust the eccentricity of the right knuckle bearing. By rotating the fine

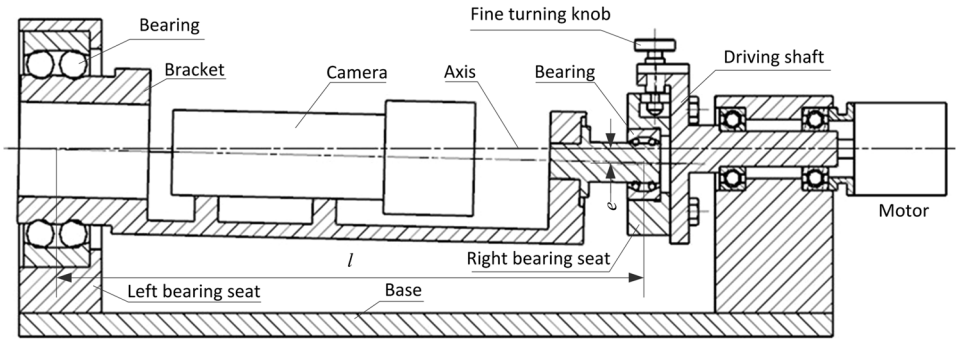

FIG. 6. Schematic of the prototype structure.

turning knob, the right knuckle bearing's position relative to the driving shaft can be adjusted.

In the design of Fig. 6, the bracket's degree of freedom around the camera's optical axis has not been constrained. The camera may rotate and wobble around its optical axis during the operation of the prototype, resulting in the phenomenon shown in Fig. 7. The mechanism that the clamp-slot matches with the ball-rod is designed to restrain the degree of freedom of the bracket around the camera axis (as shown in Fig. 8). The ball-rod is connected to the bracket, and the clamp-slot is connected to the left bearing seat. When the system is operating, the clamp-slot constrains the upper and lower degrees of freedom of the ball part so that it prevents the camera from rotating around its own axis.

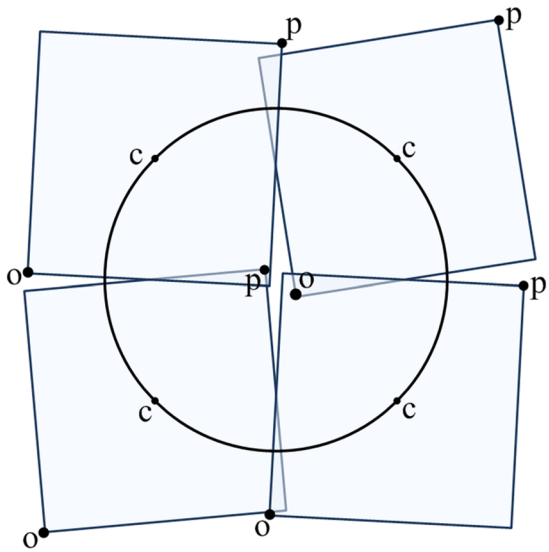

FIG. 7. Schematic of the FoV of the system when the camera deflects around its own axis.

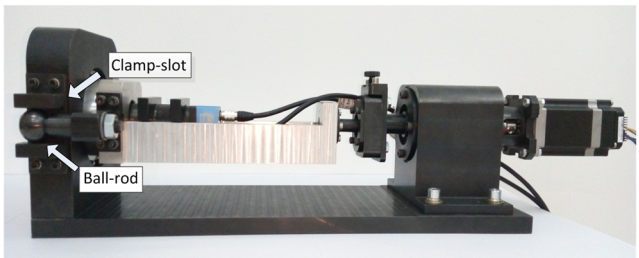

FIG. 8. Photo of the prototype.

B. Camera exposure control flow

When the system is running, the motor controls the driving shaft to rotate at a constant speed. A photoelectric encoder is installed on the driving shaft to feedback the rotation angle. As shown in Fig. 9, a digital signal processor (DSP) chip is used to collect the encoder's signals to measure the real-time rotation angle and send the trigger signal when the camera is at a specific position to expose the camera. At the same time, DSP communicates with the computer to inform the relative position of the sub-image in the field for image stitching. After each motion cycle, the computer stitches the sub-images according to their relative positions and displays them on the screen.

IV. IMAGING MOTION FEATURE ANALYSIS OF THE PROTOTYPE

As the camera is still moving when images are captured, there is a certain degree of image motion relative to the field for the image collected. This is also the main factor that influences the image quality. Because the ball-rod and clamp-slot constrains the degree of freedom of the camera around its own axis, the camera is in a translation state at any time. Figure 10

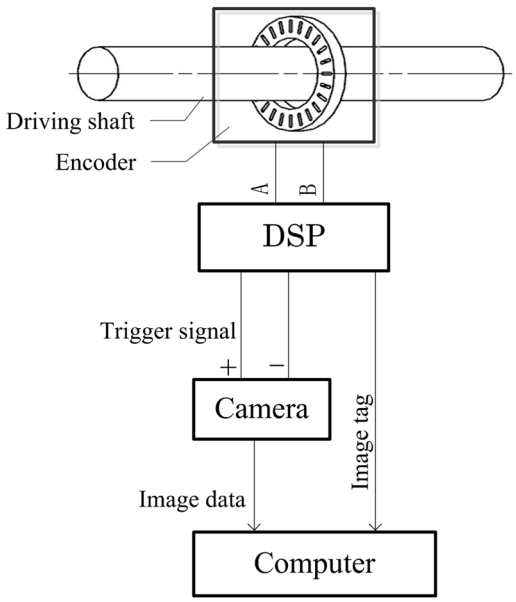

FIG. 9. Block diagram of camera exposure control flow.

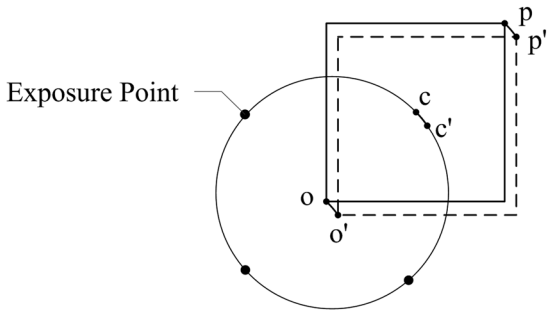

FIG. 10. Image sensor motion schematic when the camera is capturing images. Point c is the center point of the image sensor, points o and p are the corner points of the image sensor, points c', o', p' are, respectively, the position of points c, o, p when the exposure stops.

shows the motion diagram of the image sensor when the camera is capturing images. As can be seen in the figure, in any time period, each pixel of the image sensor has the same image motion relative to the field, which is a small arc.

For example, consider the center point of the image sensor c. Figure 11 shows a system diagram of the prototype at a given time, and bc is the focal length of the camera. When the system is operating, bc is always over point a. Figure 12 shows a top view of the system state diagram shown in Fig. 11. In Fig. 12, line bc moves to line b'c' when the exposure stops. Assuming the angular velocity of the conical rotation of the camera is ω, after time trace dt, point b moves to point b', point c moves to point c', and the light emitted from the object point formerly corresponding to point c is projected to point q through point b'. Then, ds is the corresponding image motion of time trace dt. According to the geometric relationship,

$$ds = ds_1 + ds_2. \tag{3}$$

As the rotational angle of the camera during dt is $\omega \times dt$, the displacement of point c is $r_1 \times \omega \times dt$ and the displacement of point b is $r_2 \times \omega \times dt$. Thus

$$ds = r_1 \cdot \omega \cdot dt + r_2 \cdot \omega \cdot dt. \tag{4}$$

Because

$$r_1 + r_2 = f \cdot \tan\left(\frac{\theta}{2}\right), \tag{5}$$

the equation can be obtained as

$$ds = f \cdot \omega \cdot \tan\left(\frac{\theta}{2}\right) \cdot dt. \tag{6}$$

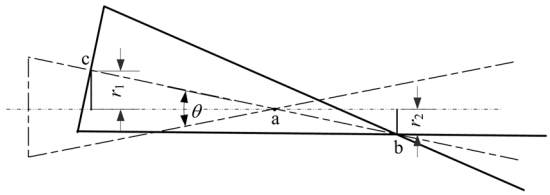

FIG. 11. State diagram of the system at a given time. In the figure, θ is the conical rotation vertex angle, point a is the conical rotation vertex, point b is the projection center of the camera, point c is the center point of the image sensor, r_1 is the distance of point c from the system axis, and r_2 is the distance of point b from the system axis.

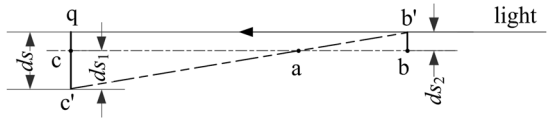

FIG. 12. Diagram showing the image motion when the camera is exposed. Point q is the projection point of the object point formerly corresponding to point c, ds_1 is the displacement of point c due to the motion of the camera, ds_2 is the displacement of point b due to the motion of the camera, and ds is the image motion corresponding to the field.

Suppose the exposure time of the camera is Δt, then the corresponding image motion Δs is

$$\Delta s = f \cdot \omega \cdot \tan\left(\frac{\theta}{2}\right) \cdot \Delta t. \tag{7}$$

V. EXPERIMENT

In the experiment, the No. 1 and No. 3 subsystems shown in Fig. 2 were simulated by adjusting the eccentricity of the camera's conic rotation and realized by 3 × 3 large field stitching. As shown in Fig. 13, the zero point of the encoder is corresponding to the left side of the FoV, so for No. 1 subsystem, the camera is, respectively, corresponding to sub-fields 4, 2, 6, 8 after rotating for 0°, 90°, 180°, 270°, and for No. 3 subsystem, the camera is, respectively, corresponding to sub-fields 1, 3, 9, 7 after rotating for 45°, 135°, 225°, 315°. The above parameters were translated into the corresponding encoder numbers and written into the DSP chip to control the camera's exposure.

In the prototype, the focal length of the camera lens was 300 mm, the resolution of the image sensor was 480 × 480, the pixel size was 6 μm, and then the angle of view of the camera was 0.78°. The preset overlap of the adjacent sub-images was 30 columns of pixels, then the resolution of the complete image was 1380 × 1380, and the overall angle of view of the system was 2.23°. When the corresponding parameters were inserted into formula (1), the conical rotation vertex angle of No. 1 and 3 subsystems, respectively, were 1.03° and 1.46°. The distance between the two knuckle bearings was 300 mm, and when it was inserted into formula (2), the eccentricity

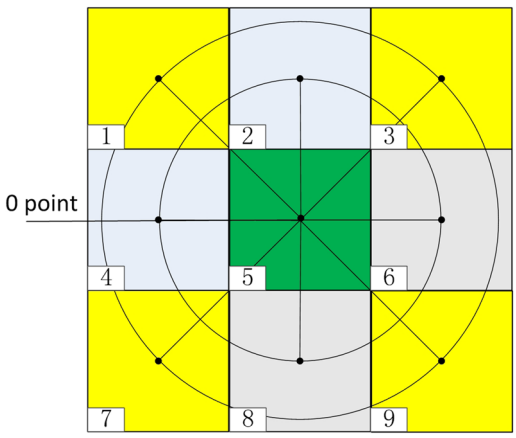

FIG. 13. Schematic of the system's FoV.

of No. 1 and No. 3 subsystems, respectively, were 2.70 mm and 3.82 mm. In the experiment, we adjusted the overlap of the sub-images by rotating the fine turning knob. Note that the fine turning knob's precision is not sufficient to adjust the overlap of the sub-images to exact 30 columns while it is not necessary to control the overlap of the sub-images precisely. For the large field imaging system, in order to cover a large field, the overlap of the sub-images is very small, and the sub-images collected cannot be registered automatically with the image stitch algorithm. So like a multi-camera array system, the sub-images are registered manually at the calibration stage, and the registration parameters are used as fixed parameters to stitch the images when the system is running. In the experiment, the rotating speed of the driving shaft was 3 rev/s and the exposure time was 250 μs; when these were inserted into formula (7), the image motions when the prototype was simulating No. 1 and No. 3 subsystems, respectively, were 13 μm and 18 μm.

Figure 14(a) shows the images collected when the prototype was simulating No. 1 and No. 3 subsystems, and the center image was collected manually after the experiment. Figure 14(b) shows the large field image after stitching manually. From the figure, we can see that the prototype is exposed to the sub-fields accurately, which proves that the large field imaging system is feasible.

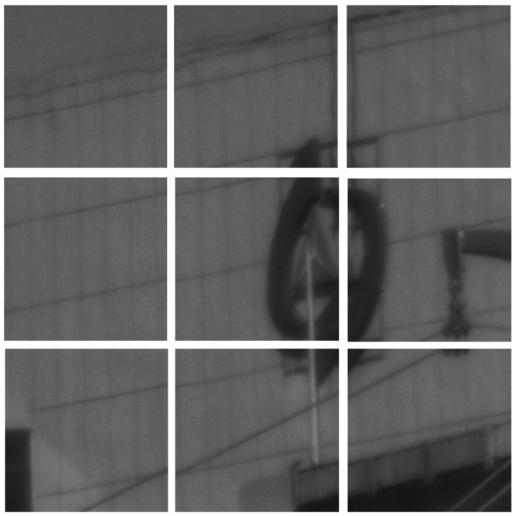

(a)

(b)

FIG. 14. (a) Sub-images collected by the prototype. (b) The complete 3 × 3 large field image after stitching.

VI. DISCUSSION

The external FoV stitching system proposed in this paper transforms the pose by controlling the camera to perform conical rotation, and it simulates a multi-camera array to image a chessboard segmented field and gets the complete field image by stitching. A similar design is a system that installs the camera onto a pan/tilt, it images a large field by controlling the camera's pointing direction to transform in a specific sequence.[20] But the system has a low frame rate and is only suitable for imaging static scenes. For a traditional remote target tracking system, it can also realize large field imaging by controlling the camera to transform its pointing direction with the turntable, and for the same reason, it cannot meet the moving target capture requirement. The imaging system proposed in this paper adds a camera conical rotation controlling mechanism between the tracking turntable and the telephoto camera to control the camera for quick pointing changes and realize a high frame rate large field scanning.

The system simulates a 3 × 3 camera array with 3 cameras. It can be seen from Fig. 4 that the space for the movement of the camera can be minimized by adjusting the position of the camera relative to point a. And since the camera has a small angle of view, the conical rotation vertex angle is small. Consequently the space for the movement of the camera is not much larger than its own volume. So the overall volume of the system is considerably smaller than that of the 3 × 3 camera array. At the same time, the use of fewer cameras helps us to reduce the weight and cost of the system. So the system has significant volume and weight advantages over the camera array, reducing the load of the turntable. The main tasks of constructing the system include the design of the camera motion control structure, the exposure control of the camera, and the processing of the image data. Considering that the above tasks can be implemented using the current mature technologies, the system is technically simple to be constructed.

VII. SUMMARY

A novel imaging system combined with an external FoV stitching method was presented in this paper to address the problem that the current telephoto camera's angle of view is too small to meet the remote target acquisition requirements. By continuously controlling the cameras to perform conical rotation, the system realizes 3 × 3 stitching and high frame rate scanning of the field. The system has significant volume and weight advantages over the multi-camera array and is suitable for mounting on the corresponding turntable. We developed an experiment prototype to verify the system. In the experiment, we used a camera with an angle of view of 0.78° and obtained a large angle of view system of 2.23°. This paper introduces the prototype design and calibration process, which provides a reference for the actual system construction.

ACKNOWLEDGMENTS

This project was supported by the Key Research Program of Frontier Science, CAS (Grant No. QYZDB-SSW-SLH014).

[1]R. S. A. R. Abdullah, A. A. Salah, A. Ismail *et al.*, "Experimental investigation on target detection and tracking in passive radar using long-term evolution signal," IET Radar Sonar Navigation **10**(3), 577–585 (2016).

[2]Y. Quan, Y. C. Li, Y. Wu *et al.*, "Moving target detection for frequency agility radar by sparse reconstruction," Rev. Sci. Instrum. **87**(9), 094703 (2016).

[3]Y. Li, P. Li, and Q. Shen, "Real-time infrared target tracking based on ℓ_1 minimization and compressive features," J. Appl. Opt. **53**(28), 6518–6526 (2014).

[4]X. M. Tang, F. Hu, M. Wang, J. Pan, S. Y. Jin, and G. Lu, "Inner FoV stitching of spaceborne TDI CCD images based on sensor geometry and projection plane in object space," Remote Sens. **6**, 6386–6406 (2014).

[5]T. Sako, T. Sekiguchi, M. Sasaki, K. Okajima, F. Abe, I. A. Bond, J. B. Hearnshaw, Y. Itow, K. Kamiya, P. M. Kilmartin, K. Masuda, Y. Matsubara, Y. Muraki, N. J. Rattenbury, D. J. Sullivan, T. Sumi, P. Tristram, T. Yanagisawa, and P. C. M. Yock, "MOA-cam3: A wide-field mosaic CCD camera for a gravitational microlensing survey in New Zealand," Exp. Astron. **22**, 51–66 (2008).

[6]D. W. Sweeney, "Overview of the large synoptic survey telescope project," Proc. SPIE **6267**, 626706 (2006).

[7]G. J. J. Winands, Z. Liu, A. J. M. Pemen, E. J. M. van Heesch and K. Yan, "Long lifetime, triggered, spark-gap switch for repetitive pulsed power applications," Rev. Sci. Instrum. **76**, 085107 (2005).

[8]V. Suntharalingam, R. Berger, S. Clark *et al.*, "A 4-side tileable back illuminated 3D-intergrated Mpixel CMOS image sensor," in *Digest of Technical Papers—IEEE International Solid-State Circuits Conference (ISSCC 2009)* (IEEE, 2009), 38–39, 39a.

[9]M. Gruber and A. Wiechert, "Ten years large format digital aerial cameras, a review," *Proceedings of the American Society for Photogrammetry and Remote Sensing Annual Conference* (2010), Vol. 1, pp. 217–221.

[10]B. Leininger, J. Edwards, J. Antoniades *et al.*, "Autonomous real-time ground ubiquitous surveillance-imaging system (ARGUS-IS)," Proc. SPIE **6981**, 69810H (2008).

[11]A. W. Lohmann, "Scaling laws for lens systems," Appl. Opt. **28**, 4996–4998 (1989).

[12]D. B. Pollock, P. J. Reardon, T. E. Rogers, C. N. Underwood, G. Egnal, B. S. Wilburn, and S. K. Pitalo, "Multi-lens array system and method," U.S. Patent 9,182,228 (10 November 2015).

[13]D. S. Kittle, D. L. Marks, H. S. Son *et al.*, "A testbed for wide-field, high-resolution, gigapixel-class cameras," Rev. Sci. Instrum. **84**(5), 053107 (2013).

[14]B. Wilburn, N. Joshi, V. Vaish, E. V. Talvala, E. Antunez, A. Barth, A. Adams, M. Horowitz, and M. Levoy, "High performance imaging using large camera arrays," ACM Trans. Graphics **24**, 765–776 (2005).

[15]G. Zhang, Z. Shao, H. Deng, and J. Ren, "Precise position synchronous control for multi-axis servo systems," IEEE Trans. Ind. Electron. **64**(5), 3707 (2017).

[16]S. L. Kovacs, "Scanning-mirror structure having a cut or a composite design to reduce deformation of the mirror face, and related system and method," U.S. patent 7,400,432 (15 July 2008).

[17]X. Liu, Z. Fang, X. Dai *et al.*, "An infrared scanning and tracking system for detecting mid-wave infrared spectral characteristics of moving targets," Appl. Spectrosc. **68**(11), 1289–1295 (2014).

[18]M. Schwalm and D. Dan, "Silicon carbide pointing mirror and telescope for the Geostationary Imaging Fourier Transform Spectrometer (GIFTS)," Proc. SPIE **5868**, 586803 (2005).

[19]X. Ma, C. Rao, and H. Zheng, "Error analysis of CCD-based point source centroid computation under the background light," Opt. Express **17**(10), 8525 (2009).

[20]R. Sargent, C. Bartley, P. Dille *et al.*, "Timelapse GigaPan: Capturing, sharing, and exploring timelapse gigapixel imagery," in *Fine International Conference on Gigapixel Imaging for Science, 2010*.